STUDY ON CONCEPTS FOR RADAR INTERFEROMETRY FROM SATELLITES FOR OCEAN (AND LAND) APPLICATIONS

Studie zu Konzepten für Radar-Interferometrie über Ozeanen (und Land) im Rahmen zukünftiger Satellitenmissionen

(KoRIOLiS)

SECTION 2: FUNDAMENTALS

Roland Romeiser and Donald R. Thompson

A fundamental requirement for SAR interferometry is sufficient correlation between the two complex images which are interferometrically combined, i.e. sufficient coherence between the backscattered signals received by the two InSAR antennas. Furthermore, the range of velocities or surface elevations which are mapped into a phase interval of 2π must be adjusted to the scales of the velocity and / or height variations to be detected.

2.1. COHERENCE

Assuming that the signal-to-noise ratio (SNR) of the radar is not a limiting factor, low correlation between two SAR images of the same scene will mainly result from low coherence of the backscattered field between the two antenna locations in space and time, which can be an effect of temporal and / or spatial decorrelation.

2.1.1. Temporal Decorrelation of the Radar Signal

In contrast to radar signals from stationary or quasi-stationary targets (land, sea ice), microwave backscatter from the moving sea surface decorrelates on very short time scales on the order of milliseconds [*Thompson*, 1989; *Thompson & Jensen*, 1993; *Plant et al.*, 1994; *Romeiser & Thompson*, 2000]. The magnitude of the autocorrelation of the backscattered field as function of the time lag τ is given by

$$\rho_t(\tau) = |r(\tau)| = \frac{1}{\sigma}\left|\int_{-\infty}^{\infty} e^{i2\pi f_D} S(f_D)\, df_D\right| \tag{2-1}$$

where r is the complex autocorrelation function, σ is the expectation value of the normalized radar backscattering cross section (NRCS), f_D is the Doppler frequency, and S is the Doppler spectrum of the backscattered signal. S is defined such that its integral yields σ. The Doppler spectrum can be considered as distribution of the Doppler frequencies in the backscattered signal in terms of their contributions to σ. It is proportional to the distribution of line-of-sight target velocities within the radar footprint and thus closely related to the surface wave spectrum [*Thompson*, 1989; *Romeiser & Thompson*, 2000].

If the backscattered field decorrelates between the acquisitions of two complex SAR amplitude images of the same scene, the images are statistically independent, and phase differences at individual pixels are random values with a uniform distribution and thus meaningless for interferometric interpretation. The correlation time or "coherence time", i.e. the time lag where ρ_t falls below a threshold value, is the reciprocal value of the Doppler bandwidth, which is basically proportional to the radar frequency and to the surface wave height [*Romeiser and Thompson*, 2000]. Examples of autocorrelation functions for L- and X-band at different wind speeds, as computed by *Romeiser and Thompson* [2000], are shown in Figure 2-1.

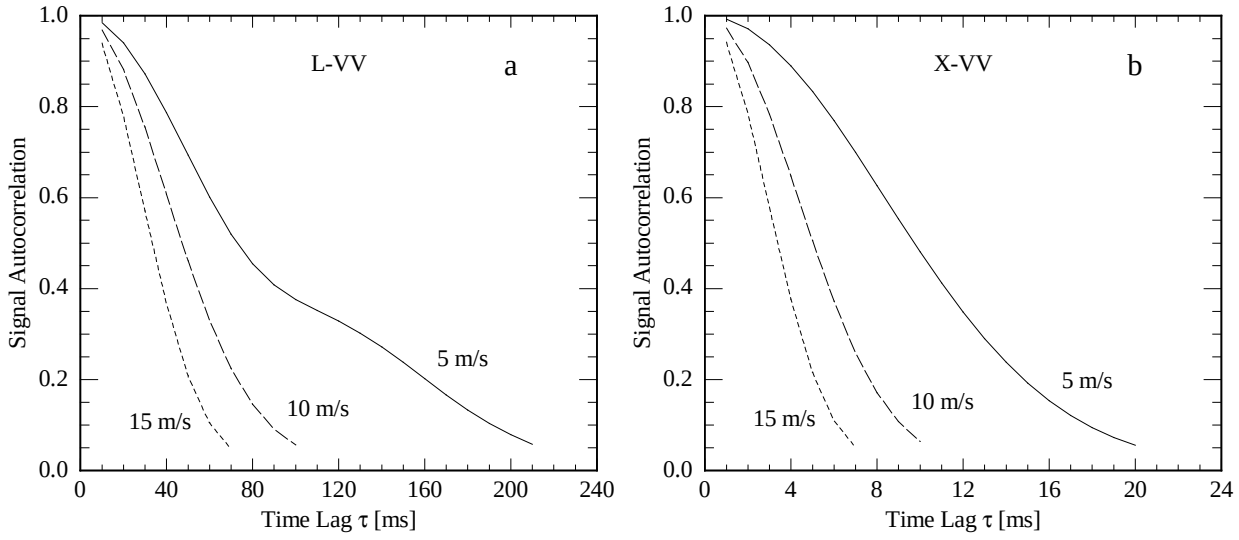

Figure 2-1: Theoretical magnitude of the autocorrelation of the backscattered field as function of InSAR time lag τ and for wind speeds of 5, 10, and 15 m/s; radar look direction = 45° from downwind; incidence angle = 60°; (a) L-band (1 GHz) VV, (b) X-band (10 GHz) VV [from Romeiser & Thompson, 2000].

Figure 2-2 shows the time lag for which ρ_t falls below 0.5 as function of radar frequency and for different wind speeds. If possible, the InSAR time lag should be shorter than this time lag. The second vertical axis of Figure 2-2 shows the equivalent along-track baseline for a typical InSAR in space with a platform velocity of 7000 m/s. According to this diagram, the along-track baseline should, if possible, not exceed approx. 30 to 50 m for X-band (10 GHz) and 300 to 500 m for L-band (1 GHz). In this context one should be aware of the fact that the effective along-track baseline is equal to the actual along-track distance between the InSAR antennas if both antennas are acting as transmitters and receivers (two monostatic SARs), but half this distance for a single-transmitter configuration (a monostatic and a bistatic SAR).

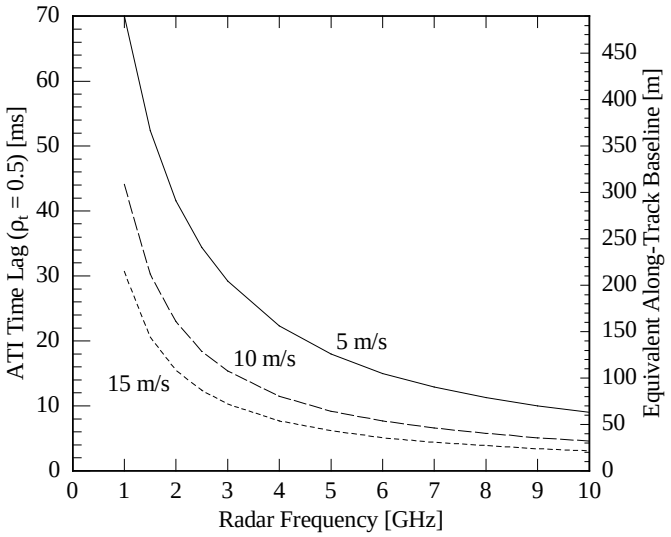

Figure 2-2: InSAR time lag τ where the autocorrelation ρ_t falls below 0.5, as function of radar frequency and for wind speeds of 5, 10, and 15 m/s; radar look direction = 45° from downwind; incidence angle = 45°; polarization = VV; second vertical axis on the right shows along-track baseline corresponding to the time lag given on the left for a typical InSAR in space (platform velocity = 7000 m/s).

2.1.2. Spatial Decorrelation of the Radar Signal

In addition to the temporal decorrelation, spatial decorrelation of the backscattered field can occur as an effect of the different incidence angles of the two antennas of an InSAR configuration with nonzero cross-track baseline. This effect is basically the same for land and ocean targets. Assuming that the transmitted SAR signal is monochromatic, one finds that the signals received by two antennas decorrelate when the number of lines of scatterers at the surface which are in phase (i.e. the number of Bragg waves) within one range resolution cell differs by more than 1. *Zebker & Villasenor* [1992] derive, with some simplifying assumptions, the following expression for the spatial correlation ρ_s of the backscattered field:

$$\rho_s = 1 - \frac{2\cos\theta\,|\delta\theta|\,\Lambda_y}{\lambda} \tag{2-2}$$

where θ is the incidence angle of one of the two SAR antennas, $\delta\theta$ is the difference between the two incidence angles, Λ_y is the ground range resolution of the radar, and λ is the radar wavelength. Using $B_\perp \approx H\,|\delta\theta|/\cos\theta$ for the cross-track baseline component normal to the direction of incidence (where H is the flight altitude of the platform), one obtains an expression for a first "critical baseline" B_{c0}, where $\rho_s = 0$:

$$B_{c0} = \frac{\lambda H}{2\Lambda_y \cos^2\theta} \tag{2-3}$$

Following this argument, interferometry appears to be impossible if $B_\perp \geq B_{c0}$. However, as shown by *Gatelli et al.* [1994], most of the spatial decorrelation can usually be compensated by taking the problem into account in the data processing. This is possible because the transmitted SAR signal is usually not monochromatic but has a finite bandwidth. Its spectrum can be filtered such that both antennas use slightly different frequency bands which correspond to a common wavenumber band at the surface, such that there is no wavelength difference anymore. One can show that this "tuning" of the radar frequency will also compensate the incidence-angle dependence of Doppler shifts associated with horizontal motions, thus it is adequate for topographic measurements and for velocity measurements by cross-track InSAR and by combined cross-track and along-track InSAR.

The absolute upper limit of the cross-track baseline, the "true" critical baseline B_c, is determined by the condition that there is no spectral overlap between the signals received by antenna 1 and antenna 2 anymore. *Gatelli et al.* [1994] obtain

$$B_c = \frac{\Delta f_y \lambda R \tan\theta}{c} \tag{2-4}$$

where Δf_y is the system's frequency bandwidth in range, $R = H/\cos\theta$ is the distance between antenna and target, and c is the speed of light. Typical critical baselines are on the order of several kilometers, thus much longer than the critical baseline B_{c0} of a monochromatic system.

Equivalent to Figure 2-2 for the temporal decorrelation, Figure 2-3 illustrates the dependence of the cross-track baseline for which ρ_s falls below 0.5 (according to (2-2) and (2-3) this is half the "monochromatic" critical baseline B_{c0}) on the radar frequency. A flight altitude of 800 km, a ground range resolution of 25 m, and incidence angles of 30° and 60° are assumed. According to this diagram, the cross-track baseline should not exceed approx. 300 to 1000 m (depending on the incidence angle) for X-band (10 GHz) and 3 to 10 km for L-band (1 GHz) if no compensation for the loss of coherence can be applied.

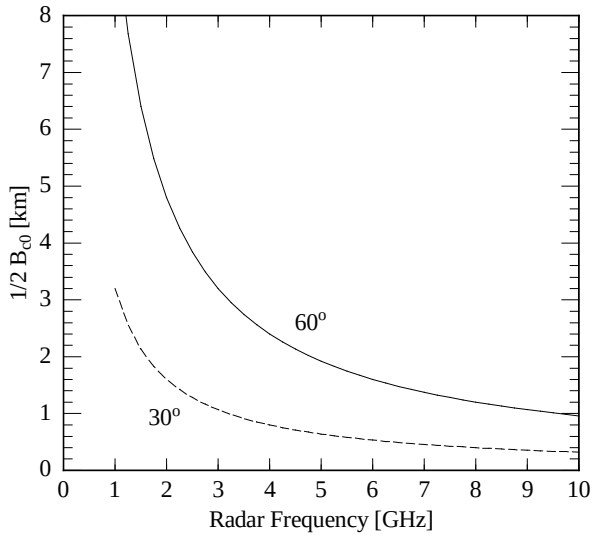

Figure 2-3: InSAR cross-track baseline B where ρ_s falls below 0.5, i.e. $B_c/2$, vs. radar frequency, for incidence angles of 30° and 60° and for a flight altitude of 800 km and a ground range resolution Λ_y of 25 m.

Another contribution to the decorrelation of cross-track InSAR images (i.e. a contribution to the uncertainty or variance of detected phase differences) results from sub-resolution-scale variations of the surface elevation. This effect corresponds to the decorrelation in time due to sub-resolution-scale variations of target velocities as described by (2-1), but it is usually small. *Zebker & Villasenor* [1992] show that the total observed correlation between the two InSAR images is the product of temporal correlation, spatial correlation, and thermal correlation (i.e. the effect of internal instrument noise). All these effects can be taken into account in our simulations.

2.2. INTERFEROMETRIC PHASE SENSITIVITY

As discussed in the previous section, the time lag between the acquisitions of the two SAR images of an InSAR system must be short compared to the decorrelation time, and the cross-track baseline component should be small compared to the critical baseline B_c, to avoid coherence problems. Perfect coherence would be obtained for vanishing along-track and cross-track baselines. However, also the detected phase differences would vanish under such conditions: As shown by *Goldstein & Zebker* [1987], a line-of-sight target velocity component v_r corresponds to an interferometric phase $\delta\varphi_v$ of

$$\delta\varphi_v = 2\pi\tau f_D = -\frac{4\pi\tau}{\lambda} v_r \tag{2-5}$$

where τ is the InSAR time lag. For the ocean surface with pronounced sub-resolution-scale variations in the velocity field and a corresponding Doppler spectrum of the backscattered signal (instead of one discrete Doppler frequency f_D), this expression must be replaced by

$$\delta\varphi_v = \arg(R_P) = \arg\left(\frac{1}{\sigma_P} \int_{-\infty}^{\infty} e^{i2\pi f_D} S_P(f_D) df_D \right) \tag{2-6}$$

[*Thompson & Jensen*, 1993], where $S_P(f_D)$ is the Doppler spectrum of contributions to the backscattered signal which are mapped into the same pixel and σ_P is its integral. Due to a strong correlation between line-of-sight velocity and NRCS variations along ocean waves, the mean Doppler offset and, thus, the InSAR phase according to (2-6) can be significantly different from the Doppler offset or InSAR phase according to (2-5) which would be obtained for the spatially averaged line-of-sight velocity.

While InSAR phases associated with line-of-sight velocities are proportional to the time lag τ and thus to the along-track baseline of the InSAR system, the mapping of surface elevations is determined by the horizontal and vertical cross-track baseline components B_y and B_z: One obtains for the interferometric phase $\delta\varphi_e$ associated with a surface elevation ζ

$$\delta\varphi_e = \frac{4\pi}{\lambda} \left(\cos\theta - \frac{H + B_z}{\sqrt{(H\tan\theta - B_y)^2 + (H + B_z)^2}} \right) \zeta \tag{2-7}$$

Similar to (2-6), also this expression should be replaced by an integration over power-weighted contributions from different elevation levels to account for sub-resolution-scale variations of ζ on a realistic ocean surface. However, the relative contribution of correlated surface elevation and NRCS variations to $\delta\varphi_e$ is small compared to the above-mentioned contribution of wave motion effects to $\delta\varphi_v$, since the surface elevation and the NRCS are, for typical incidence angles, out of phase by almost $\pi/2$.

It is important to adjust the along-track and cross-track baselines of an InSAR system, thus its sensitivity, to the scales of the expected variations of line-of-sight velocities and / or surface elevations to be detected. If the baselines are too small, phase differences associated with significant changes in the surface current or elevation can be below the noise level. Large baselines, on the other hand, are not favorable because of decreasing correlation of the received signals and because of phase wrapping effects and corresponding ambiguities that occur when the range of velocities or elevations of interest is mapped into a phase interval on the order of 2π or more. Figure 2-4 illustrates the relation between the horizontal velocity interval mapped into a phase difference interval of 2π and the InSAR time lag / along-track baseline, and Figure 2-5 illustrates the corresponding relation between elevation interval and cross-track baselines. Hatched areas indicate a risk of a correlation below 0.5 (cf. Figures 2-2 and 2-3) and a risk of phase wrapping, i.e., a risk of mapping realistic velocity or elevation ranges into a phase interval of more than 2π, which leads to ambiguities. We assume that realistic velocities and elevations should usually be within a range of ±2 m/s and ±25 m, respectively.

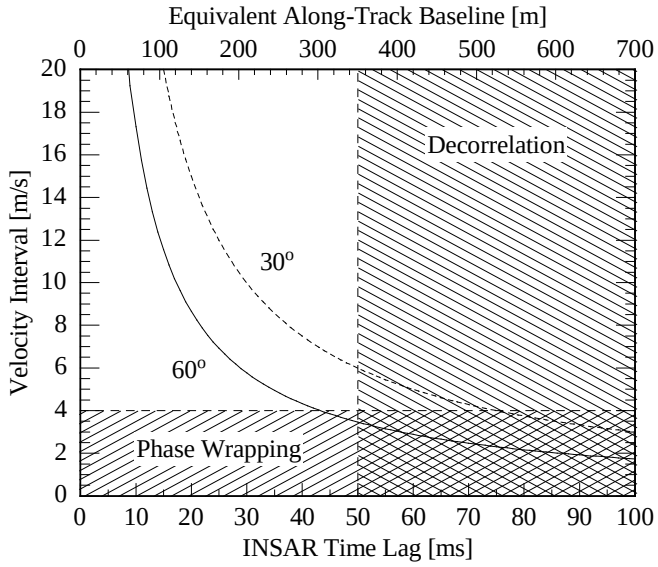

Figure 2-4: Relation between InSAR time lag τ / equivalent along-track baseline of a spaceborne InSAR (velocity = 7000 m/s) and range of horizontal target velocities which is mapped into an interferometric phase interval of 2π, for incidence angles of 30° and 60° and a radar frequency of 1 GHz (L-band). Hatched areas indicate occurrence of decorrelation and phase wrapping. The same diagram is valid for radar frequencies F GHz with time lags and along-track baselines divided by F.

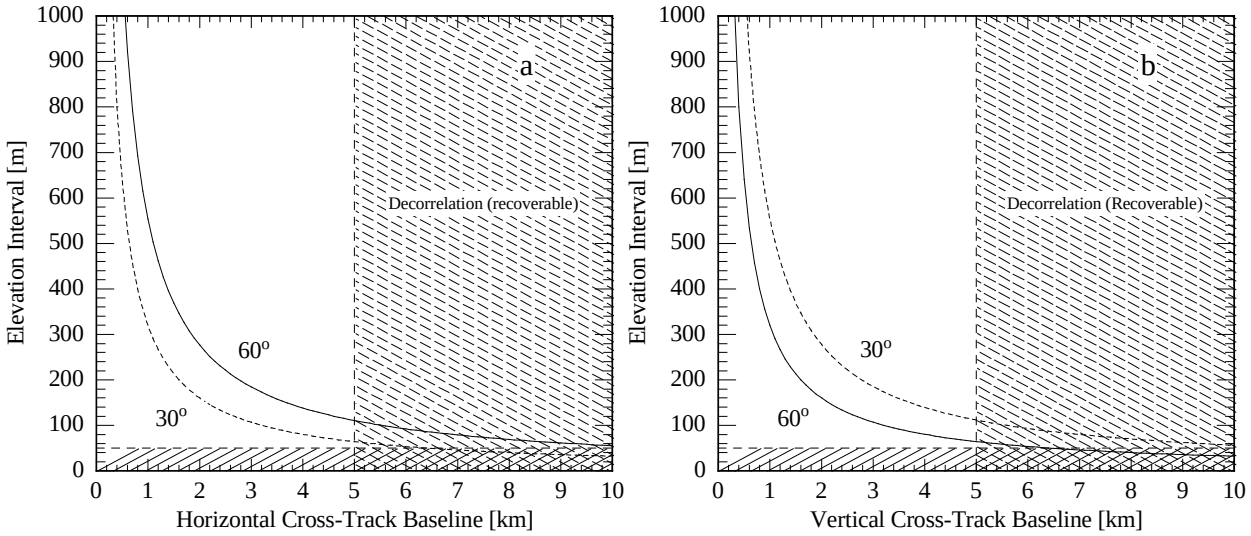

Figure 2-5: Relation between cross-track baselines of a spaceborne InSAR (H = 800 km) and range of target elevations which is mapped into a phase interval of 2π, for incidence angles of 30° and 60° and a radar frequency of 1 GHz (L-band); (a) assuming a purely horizontal cross-track baseline, (b) assuming a purely vertical cross-track baseline. Hatched areas indicate occurrence of decorrelation (for a ground range resolution of 25 m and assuming that no compensation is applied – see 2.1.2) and phase wrapping. The same diagrams are valid for radar frequencies F GHz with baselines divided by F.

While the diagrams depict that useful along-track and cross-track baselines differ by about an order of magnitude, we find for both applications that decorrelation becomes the limiting problem before phase wrapping occurs. Accordingly, one should usually choose the longest baselines that guarantee reasonable correlation in order to obtain maximum sensitivity of an InSAR system for velocity and / or elevation measurements. For the L-band example, an along-track baseline of about 350 m should result in reasonable correlation and in unambiguous mapping of a velocity range of 6 m/s into the phase interval of 2π (for an incidence angle of 30°). If InSAR phases can be determined with an accuracy of 1°, this corresponds to a velocity resolution of 0.017 m/s. Under the same conditions, a horizontal cross-track baseline of 5000 m corresponds to an unambiguous elevation interval of 64 m and a height resolution of 0.18 m. These accuracy figures are promising, but we will show in the next section that they are only valid for mean values over many pixels, while low coherence can reduce the accuracy of velocity or elevation estimates for individual pixels enormously.

2.3. PHASE STATISTICS

A comprehensive mathematical discussion on the statistics that apply to the phase differences between two SAR images can be found in the book by *Middleton* [1960], which is also cited, for example, in the JHU/APL report by *Thompson & Jensen* [1991] and in the paper by *Chapman et al.* [1994]. Despite the complex analytical expressions which are obtained for the probability density function (PDF) of InSAR phases, the actual processes whose effect is described by these expressions are relatively simple and can be understood and simulated numerically without major effort.

A fundamental assumption is that the real and imaginary parts of the backscattered signals received by the two InSAR antennas at slightly different times and / or incidence angles are jointly Gaussian quantities. The correlation between the two complex signals is given by a complex autocorrelation function, whose magnitude is essentially the product of temporal and spatial correlation factors ρ_t and ρ_s as given in section 2.1 (and a thermal noise factor, which will be neglected in the following), and whose phase is the expectation value of the InSAR phase to be detected.

For small baselines, the magnitude of the autocorrelation function, i.e. the coherence, is close to 1, and a Gaussian distribution of the InSAR phase is obtained. With increasing baselines, thus decreasing coherence, this distribution becomes wider but remains essentially Gaussian until its width (the range of phases where the PDF is significantly larger than 0) approaches 2π. At this point the phases of different realizations of the InSAR image can range from $-\pi$ to π, and a further increase of the width of the distribution results in a kind of "phase wrapping" effect, i.e. an addition of different "branches" of the Gaussian PDF which are mapped into a common 2π interval. This effect is responsible for the difficulties to derive a simple analytical expression for the total PDF. It is illustrated by Figure 2-6.

One can define the "equivalent RMS variability" γ of the unwrapped Gaussian PDF as a measure of the width of the phase distribution. For the following discussion this is a more convenient quantity than the RMS variability of the actual phase distribution, which is limited to an interval of 2π. Figure 2-7 shows the relation between γ and the total coherence ρ. For small values of γ, where phase wrapping is negligible, γ is equal to the actual standard deviation of the detected InSAR phases.

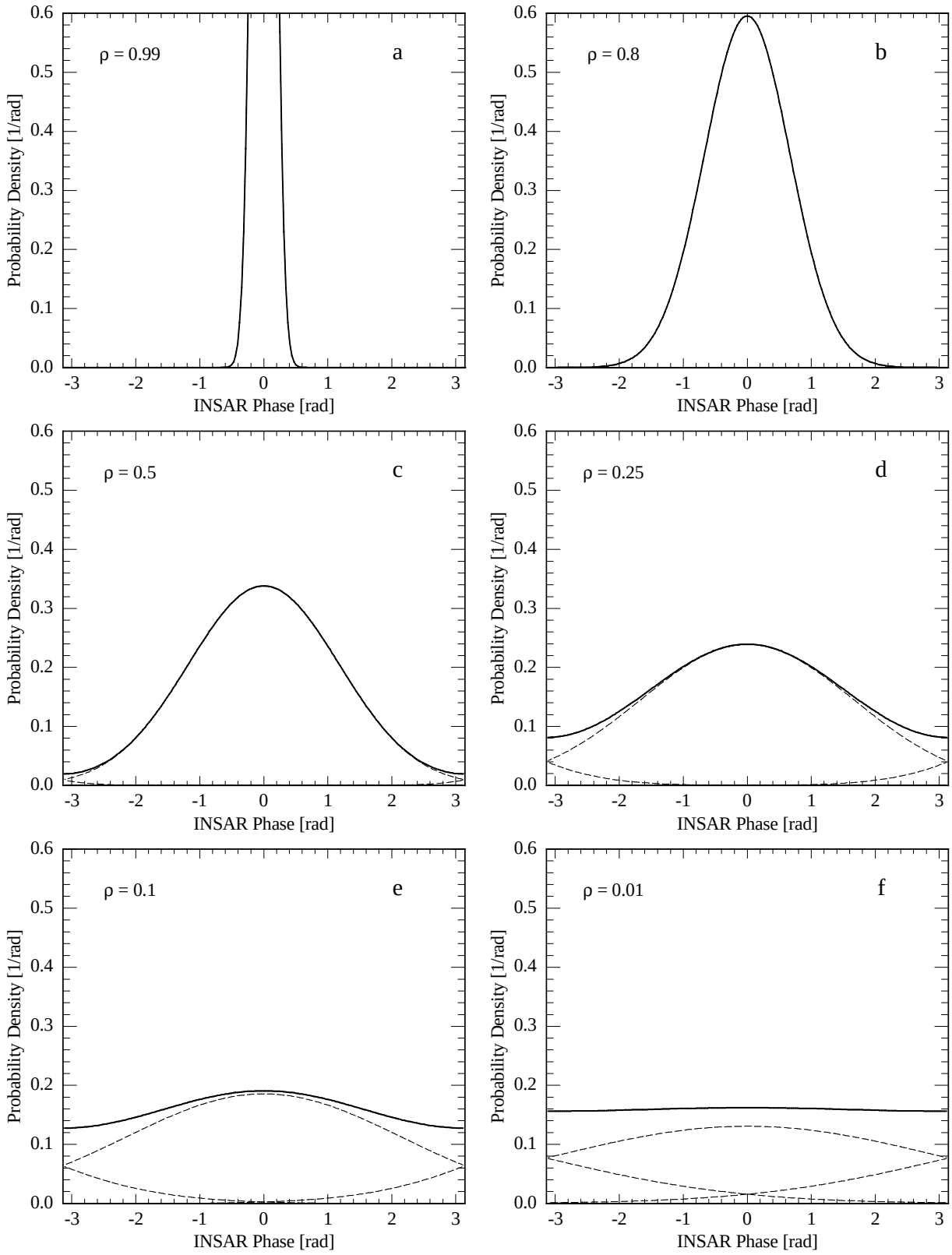

Figure 2-6: Illustration of the composition of the PDF of InSAR phases (bold solid line) as sum of different branches of a Gaussian PDF wrapped around a periodic 2π interval (dashed lines) for coherences of (a) 0.99, (b) 0.8, (c) 0.5, (d) 0.25, (e) 0.1, and (f) 0.01; mean phase is 0 in this example.

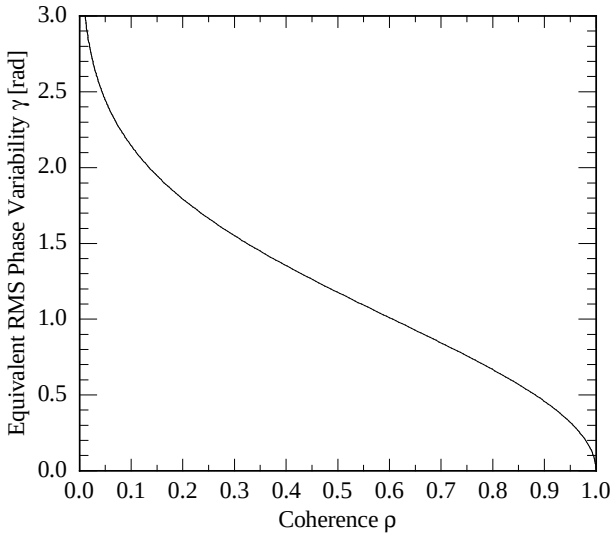

Figure 2-7: Relation between the coherence ρ of InSAR data and the "equivalent RMS variability" γ of the corresponding unwrapped Gaussian PDF.

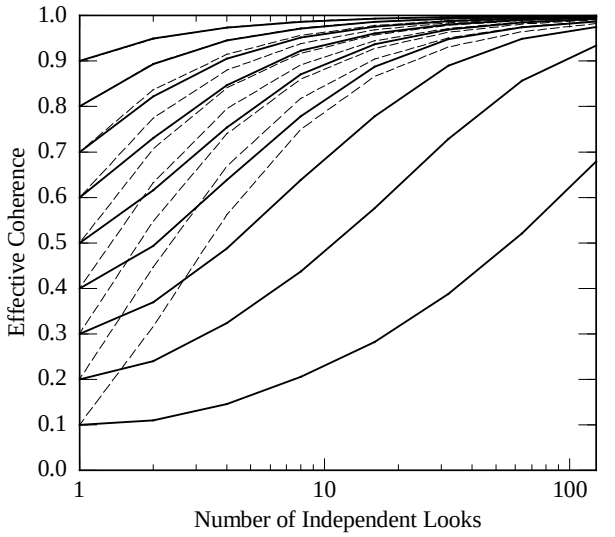

Figure 2-8: Increase of the "effective coherence" of InSAR data with the number of averaged independent samples, for initial (single look) coherence values of 0.1, 0.2, ..., 0.9 (bold solid lines). For comparison, dashed lines show results which would be obtained by averaging over samples of corresponding unwrapped Gaussian distributions (cf. Figures 2-6, 2-7).

The statistics discussed so far applies to single-look SAR images, i.e. single realizations of full-resolution images. It is possible to reduce the phase noise in such data by averaging over a number of independent samples, i.e. pixel values. For example, averaging a SAR intensity image over N pixels reduces the RMS speckle noise by a factor $1/\sqrt{N}$ (while the spatial resolution gets worse by a factor $\sqrt{N}$), since the variance of a sum of independent quantities is equal to the sum of their individual variances. Unfortunately this rule cannot be applied to the variances of the equivalent Gaussian PDFs of InSAR phase noise, γ^2, as defined above. Figure 2-8 shows for a few initial values of ρ how the "effective coherence" of InSAR images can be improved by averaging and how the results differ from those that would be obtained by averaging samples of corresponding unwrapped Gaussian distributions. Examples of simulated phase images with different effective coherences and numbers of independent samples, as well as the corresponding phase PDFs, are shown in Figure 2-9.

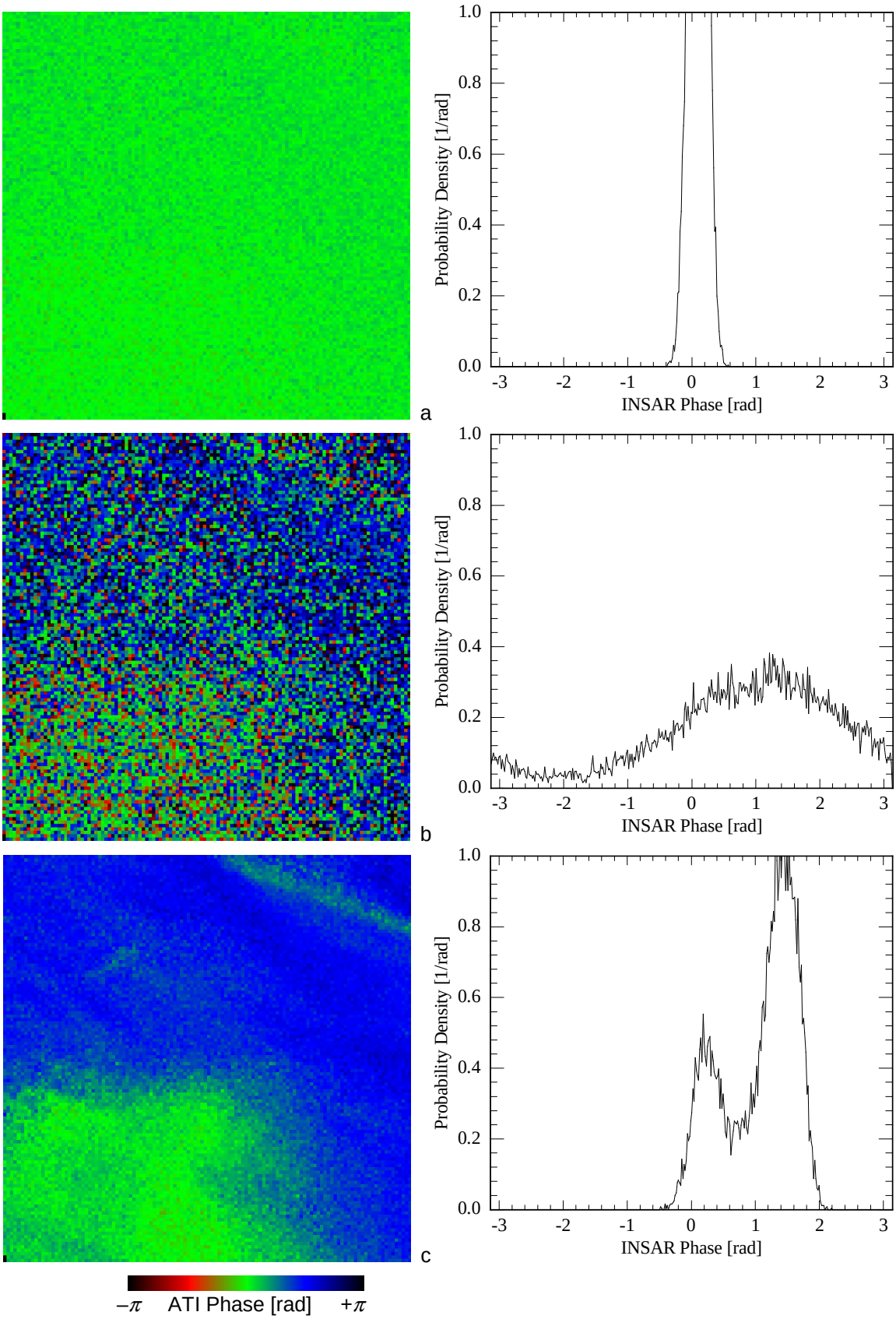

Figure 2-9: Simulated ATI phase image of a current field (left) and its phase distribution (right) for different time lags and numbers of looks; (a) with a very short time lag, phase noise is low (mean coherence = 0.99), but phase signatures are very small and likely to disappear in instrument noise; (b) a longer time lag leads to more pronounced phase signatures, but also to increased noise (mean coherence = 0.50); (c) same as (b), but assuming that each pixel value is obtained by averaging over 100 subsamples – a current pattern becomes clearly visible.

2.4. SUMMARY

Our main findings on fundamental principles and requirements for the use of spaceborne interferometric synthetic aperture radar for oceanic applications can be summarized as follows:

- The radar backscatter from the ocean decorrelates very fast. For any kind of interferometry with two complex SAR images, the lag between the acquisition times must be short compared to the decorrelation time of the signal. Over the ocean, the maximum acceptable time lag is on the order of 50 to 100 milliseconds for L-band (1 GHz) and 5 to 10 milliseconds for X-band (10 GHz).
- Also spatial decorrelation between the two incidence angles of a cross-track interferometric SAR can become a problem, but this effect can be compensated by filtering the signals such that both radars use a common horizontal wavenumber band (i.e. the same Bragg waves) in the illuminated region.
- The sensitivity of along-track and cross-track interferometric SARs to variations in the surface current and elevation increases with the along-track and the cross-track baseline, respectively. If the baselines are too short, small variations in the surface current or in the surface elevation cannot be detected. If the baselines are very long, the range of velocities or elevations mapped into a phase interval of 2π can become narrower than the actual range of velocities or elevations in the test area, and phase wrapping will occur and make the data interpretation difficult. We find that optimum along-track and cross-track baselines for oceanic applications are near the coherence limit, that is, the longest baselines which ensure sufficient coherence (without compensation) should be used because they also provide the best possible sensitivity without phase wrapping problems.
- Phase noise in ATI images with low coherence can be reduced by averaging over a number of pixels, but the effectiveness of this noise reduction decreases with decreasing coherence.

REFERENCES

Chapman, R.D., B.L. Gotwols, and R.E. Sterner II, On the statistics of the phase of microwave backscatter from the ocean surface, *J. Geophys. Res.*, *99*, 16,293-16,301, 1994.

Gatelli, F., A.M. Guarnieri, F. Parizzi, P. Pasquali, C. Prati, and F. Rocca, The wavenumber shift in SAR interferometry, *IEEE Trans. on Geosci. and Remote Sensing*, *32*, 855-865, 1994.

Goldstein, R.M., and H.A. Zebker, Interferometric radar measurement of ocean surface currents, *Nature*, *328*, 707-709, 1987.

Middleton, D., *An Introduction to Statistical Communications Theory*, McGraw-Hill, New York, 1960.

Plant, W.J., E.A. Terray, R.A. Petitt, Jr., W.C. Keller, The dependence of microwave backscatter from the sea on illuminated area: Correlation times and lengths, *J. Geophys. Res.*, *99*, 9705-9723, 1994.

Romeiser, R., and D.R. Thompson, Numerical study on the along-track interferometric radar imaging mechanism of oceanic surface currents, *IEEE Trans. on Geosci. and Remote Sensing*, *38-II*, 446-458, 2000.

Thompson, D.R., Calculation of microwave Doppler spectra from the ocean surface with a time-dependent composite model, in *Radar Scattering from Modulated Wind Waves*, edited by G.J. Komen and W.A. Oost, Kluwer Academic Publishers, Dordrecht, Netherlands, 27-40, 1989.

Thompson, D.R., and J.R. Jensen, *SAR Interferometry Models Applied to Loch Linnhe Internal Waves*, *JHU/APL Report S1R-91U-031*, 49 pp., Johns Hopkins University / Applied Physics Laboratory, Laurel, MD, USA, 1991.

Thompson, D.R., and J.R. Jensen, Synthetic aperture radar interferometry applied to ship-generated waves in the 1989 Loch Linnhe experiment, *J. Geophys. Res.*, *98*, 10,259-10,269, 1993.

Zebker, H.A., and J. Villasenor, Decorrelation in interferometric radar echoes, *IEEE Trans. on Geosci. and Remote Sensing*, *30*, 950-959, 1992.